

1
2

3
4

5
6
7
8
9
10
11

Ionospheric Plasma IRregularities - IPIR - data product based on data from the Swarm satellites

Yaqi Jin¹, Daria Kotova¹, Chao Xiong^{2,3}, Steffen Brask¹, Lasse B. N. Clausen¹, Guram Kervalishvili², Claudia Stolle^{2,4}, and Wojciech J. Miloch¹

¹Department of Physics, University of Oslo, Box 1048 Blindern, 0316 Oslo, Norway

²Helmholtz Centre Potsdam, GFZ German Research Centre for Geosciences, Telegrafenberg, 14473

Potsdam, Germany

³Now at Department of Space Physics, Electronic Information School, Wuhan University, 430072 Wuhan, China

⁴Now at Leibniz Institute of Atmospheric Physics e.V. at the University of Rostock, Schloßstraße 6, 18225 Kühlungsborn, Germany

12
13
14
15
16
17

Key Points:

- IPIR is a new Swarm data product that characterises ionospheric plasma irregularities
- Plasma irregularity parameters are assigned to different geomagnetic regions
- IPIR allows for both detailed case studies and global statistical studies of ionospheric plasma variability

Corresponding author: W. J. Miloch, w.j.miloch@fys.uio.no

Abstract

Ionospheric plasma irregularities can be successfully studied with the Swarm satellites. Parameters derived from the in situ plasma measurements and from the topside ionosphere total electron content provide a comprehensive dataset for characterising plasma structuring along the orbits of the Swarm satellites. The Ionospheric Plasma IRregularities (IPIR) data product summarizes these parameters and has already been used in studies related to structuring and variability of ionospheric plasma. We provide a detailed description of the algorithms behind the IPIR data product and demonstrate its use for ionospheric studies.

1 Introduction

The dynamics of ionospheric plasma are coupled to different processes in the solar wind, magnetosphere, thermosphere and lower atmosphere. This complex coupling often gives rise to plasma instabilities and turbulence, which lead to structuring in the ionospheric plasma (Hasegawa et al., 2004; Kintner & Seyler, 1985; Moen et al., 2013). The resulting irregularities in the plasma density can impact the propagation of radio waves, leading to radar echoes, impacting communication services, or affecting trans-ionospheric radio signals, such as those of the Global Navigation Satellite Systems (GNSS) (Kintner et al., 2007). Thus, ionospheric plasma irregularities are an important aspect of the space weather system. They are also a space weather risk, which can be crucial for the ground-based operations that rely on precise positioning with the GNSS systems, such as with the GPS, GLONASS, Galileo, or Beidou satellite constellations (Pi et al., 1997; Jakowski et al., 2012).

The occurrence and strength of plasma irregularities are related to the geomagnetic activity, and depend on the geomagnetic region of interest. The Interplanetary Magnetic Field (IMF) and solar wind conditions control the energy input into the magnetosphere-ionosphere-thermosphere (MIT) system (Borovsky, 2021). This is notable at high latitudes, with increased auroral activity and related phenomena during prolonged periods of the IMF B_z negative, which facilitates the magnetic reconnection on the dayside magnetosphere, and thus allows for the energy input into the MIT system (Cowley & Lockwood, 1992; Lockwood & Carlson, 1992; Carlson, 2012). Such phenomena as the polar cap patches (PCPs), auroral blobs, or auroral electrojets are subject to various plasma instabilities and hence to plasma structuring (Jin et al., 2014, 2015, 2016; van der Meeren et al., 2015). Significant plasma structuring is also present in the equatorial ionosphere, where it is manifested within the Equatorial spread F (Woodman, 2009). In the post-sunset sector, the Rayleigh-Taylor instability impacts the ionospheric F-layer, which is also reflected in the equatorial bubbles (Woodman & La Hoz, 1976; Farley et al., 1970). Thus, the polar cap, auroral oval, and post-sunset equatorial regions are characterised by the most structured plasma densities (Basu et al., 2002; Jin et al., 2020). This is also seen in the statistical maps of ionospheric scintillations of transionospheric radio waves, which assign strongest scintillations to these regions (Basu et al., 1988).

Characterising and monitoring of structuring in the ionospheric plasma density is thus of both scientific and practical interests. The understanding of ionospheric plasma response to external drivers, such as the solar wind, IMF, or gravity waves, will shed more light onto coupling processes in the MIT system and can contribute to the global ionospheric models (Wood & et al., 2021). On the other hand monitoring of the plasma irregularities at different scales is important for development of the operational space weather services related to the quality of transionospheric radio signals (Jakowski et al., 2005).

The in situ measurements of plasma structuring can be successfully done with scientific satellites in the low-Earth-orbit (LEO). In particular the Swarm constellation

of three satellites in the polar orbits has been used to successfully address several aspects of the plasma structuring in the ionosphere (Stolle et al., 2013). Swarm satellite data have for example been used for detecting the polar cap patches (Spicher et al., 2017), equatorial bubbles (Park et al., 2013), or field aligned currents (Ritter et al., 2013; Lühr et al., 2015). Several years of operations allow for a comprehensive study of the processes and structuring in the ionospheric plasma and assessing its variability. In this paper, we present a Level-2 IPIR¹ data product that has been developed for the purpose of comprehensive characterisation of plasma irregularities and structuring in the ionosphere, and demonstrate its use on a case study.

2 Swarm satellites

Swarm is the European Space Agency’s (ESA) constellation mission (Friis-Christensen et al., 2006). Three identical satellites (Swarm A, B, C) were launched into near-polar orbits on November 22, 2013. The satellites were initially in the pearl-of-strings configuration, which allowed for example for studying the evolution of PCPs (Spicher et al., 2015). Until April 2014 the orbits drifted in such a way that they reached final configuration. The Swarm A and C satellites are at approximately 460 km altitude, while Swarm B is at a higher orbit, ca. 510 km. The orbits can be adjusted so that different science goals can be achieved. Collectively, due to the slow drift of orbital planes, the Swarm satellites currently provide a coverage of all local times within approximately 4-5 months, thus allowing for long term statistical studies. Swarm A and C are closely located, which facilitates determining electric currents in the ionosphere. While the main objectives of the Swarm mission have been the understanding of the dynamics of the core of the Earth, mantle conductivity and magnetic field of the Earth, and the ionospheric current systems (Olsen et al., 2013), the mission has been successfully used for ionospheric and space weather related research (see e.g., Wood and et al. (2021) and references therein).

The payload of each of the Swarm satellites is identical and consists of the Absolute Scalar Magnetometer (ASM), Vector Field Magnetometer (VFM), Star Tracker (STR), Electric Field Instrument (EFI), GPS Receiver (GPSR), Laser Retro-Reflector (LRR) and Accelerometer (ACC). For the purpose of the IPIR dataset, the main instruments used are the EFI and GPSR. EFI consists of a thermal ion imager and two Langmuir probes, and it allows for determining the ion density, ion drift velocity and the electric field at the front panel of the satellite, and the electron plasma density and temperature (Buchert et al., 2015; Knudsen et al., 2017). IPIR also uses data from GPSR for calculating the total electron content (TEC) of the topside ionosphere and related parameters (Xiong et al., 2018). Finally, the magnetometer data are used for detecting ionospheric currents (Lühr et al., 2015) and equatorial bubbles (Park et al., 2013; Rodríguez-Zuluaga et al., 2017).

3 Data Product and Availability

IPIR is a Level 2 (L2) data product, which is derived from several Swarm L1b and L2 data products through data assimilation and processing. It builds upon the following Swarm products: the plasma density (from EF1x_LP_1B), Ionospheric Bubble Index (IBI, from IB1xTMS_2F), auroral boundaries detection based on field aligned currents (from AOBx_FAC_2F), topside-ionosphere total electron content (TEC, from TECxTMS_2F), as well as Polar Cap Products (Spicher et al., 2017). These data products are further processed and incorporated into the IPIR dataset which is denoted in the ESA system as IPDxIRR_2F. The IPIR dataset is freely available at the ESA

¹ IPIR stands for "Ionospheric Plasma IRregularities"

Swarm dissemination servers². The data is provided with the temporal resolution of 1Hz along entire orbits of the Swarm satellites. The dataset includes time series of local plasma conditions, including background density and total electron content, and derived parameters which characterise plasma structuring. These time series are assigned to geomagnetic regions: equatorial, mid-latitudes, auroral latitudes, and the polar cap regions. The mid/high latitudes and the polar cap region boundaries are dynamically determined. The whole IPIR dataset consists of 29 entries which are summarised in Table 1.

IPIR has been incorporated into the VirES for Swarm platform³. VirES is an open access interactive interface for data manipulation and retrieval of ESA Swarm mission data products. Using this interface, one can over-plot different datasets and quickly identify regions of interests, as well as import relevant numerical data values for further analysis.

4 Processing algorithms

The electron density (n_e) and electron temperature (T_e) data are taken from the L1b dataset: EFIX_LP_1B. The background density ($n_{e,b}$), foreground density ($n_{e,f}$), the polar cap patch flag (PCP_flag), and the electron density gradient near the edge of a PCP are processed with the same algorithm as in the Polar Cap Products (Spicher et al., 2017). The background density is calculated from n_e using a 35th percentile filter of 551 data points, which corresponds to approximately 2000 km for 2 Hz data at the Swarm orbital speed of ~ 7.5 km/s. The foreground density is calculated from n_e using a 50th percentile filter of 7 data points (~ 25 km). PCP_flag indicates whether the measurements are taken within the PCP, which is here defined as an increase in density within the polar cap by a factor of 2 with respect to the background: $n_{e,f}/n_{e,b} \geq 2$ (Crowley, 1996). PCP_flag is set to non-zero values, provided that the extent of the density increase is larger than 100 km. The edges of the PCP are also investigated, and defined as when $n_{e,f}$ drops to 30% of the average value of $n_{e,f}$ within the identified patch. The numerical values of PCP_flag are the following: 0 - if the measurement is taken outside PCP, 1 - the PCP edge (when no plasma velocity is available and trailing/leading edges can not be distinguished), 2 - leading edge of PCP, 3 - trailing edge of PCP, 4 - center of PCP. Grad_Ne_at_PCP_edge parameter is the electron density gradient calculated over the edge of a PCP which is non-zero only on the edges of PCPs. More details on the processing algorithm of the Polar Cap Products, their justifications, and example of use can be found in Spicher et al. (2017).

The 2Hz electron density data is used to derive parameters which characterise variations in the plasma density. The electron density gradients are calculated in the running windows of 27, 13, and 5 data points, which for Swarm correspond to spatial scales of 100, 50, and 20 km, respectively. The gradients are calculated using a linear regression to the data over certain time intervals, as illustrated in Fig. 1.

Another parameters characterising variations in the plasma density irregularities are the rate of change of density (ROD) and the rate of change density index (RODI). ROD is the time derivative of electron plasma density:

$$\text{ROD}(t) = \frac{n_e(t + \Delta t) - n_e(t)}{\Delta t}, \quad (1)$$

where $\Delta t = 0.5$ s, as we use 2 Hz data to account also for small scale fluctuations. While ROD is defined in the temporal domain, it can also be translated into spatial

² Data product is available at <https://swarm-diss.co.esa.int>, and the reference documentation can be found at <https://earth.esa.int/web/guest/missions/esa-co-missions/swarm/key-documentation>

³ <https://vires.services>

Table 1. Summary of parameters in the IPIR (IPDxIRR_2F) dataset.

Name	Description	Unit
Timestamp	CDF epoch of the measurement	deg
Latitude	Position in ITRF – Latitude	deg
Longitude	Position in ITRF – Longitude	deg
Radius	Position in ITRF – Radius	m
Ne	Electron density, n_e ; downsampled to 1Hz	cm^{-3}
Background_Ne	Background electron density, $n_{e,b}$	cm^{-3}
Foreground_Ne	Foreground electron density, $n_{e,f}$	cm^{-3}
Te	Electron temperature, T_e ; downsampled to 1Hz	K
PCP_flag	The polar cap patch flag	-
Grad_Ne_at_100km	The electron density gradient over 100 km based on 2Hz data	cm^{-3}/m
Grad_Ne_at_50km	The electron density gradient over 50 km based on 2Hz data	cm^{-3}/m
Grad_Ne_at_20km	The electron density gradient over 20 km based on 2Hz data	cm^{-3}/m
Grad_Ne_at_PCP_edge	The electron density gradient calculated on the edge of PCP when PCP detected	cm^{-3}/m
ROD	Rate Of change of Density, dn/dt	cm^{-3}/s
RODI10s	Rate Of change of Density Index (RODI) over 10 seconds	cm^{-3}/s
RODI20s	Rate Of change of Density Index (RODI) over 20 seconds	cm^{-3}/s
delta_Ne10s	Fluctuation amplitudes over the baseline of 10 seconds	cm^{-3}
delta_Ne20s	Fluctuation amplitudes over the baseline of 20 seconds	cm^{-3}
delta_Ne40s	Fluctuation amplitudes over the baseline of 40 seconds	cm^{-3}
num_GPS_satellites	Total number of tracked GPS satellites above 20 degrees elevation angle	-
mVTEC	Median of VTEC from all available GPS satellites above 30 degrees	TECU
mROT	Median of Rate Of TEC (ROT) from all available GPS satellites above 30 degrees	TECU/s
mROTI10s	Median of Rate Of TEC Index (ROTI) over 10 seconds from all available GPS satellites above 30 degrees	TECU/s
mROTI20s	Median of Rate Of TEC Index (ROTI) over 20 seconds from all available GPS satellites above 30 degrees	TECU/s
IBI_flag	Plasma Bubble Index, copied from the level-2 Ionospheric Bubble Index product, IBIXTMS_2F	-
Ionosphere_region_flag	Determining the geomagnetic region where the measurement was taken (0: equator, 1: mid-latitudes; 2: auroral oval; 3: polar cap)	-
IPIR_index	Determining the level of fluctuations in the ionospheric plasma density	-
Ne_quality_flag	Quality flag for the n_e data and the derived data	-
TEC_STD	Standard deviation of VTEC from GPS satellites	TECU

domain, where it might correspond to density gradients at scales of $\sim 3 - 4$ km when accounting also for relative motion of the Swarm satellite and plasma. RODI is the standard deviation of ROD in a given running window:

$$\text{RODI}(t) = \sqrt{\frac{1}{N-1} \sum_{t_i=t-\Delta t/2}^{t_i=t+\Delta t/2} |\text{ROD}(t_i) - \overline{\text{ROD}}|^2}, \quad (2)$$

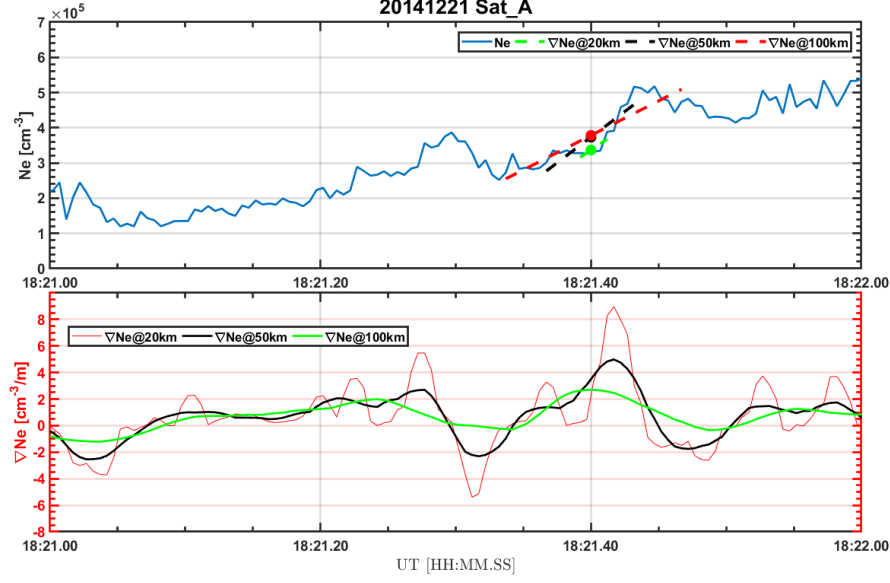


Figure 1. Example of calculating density gradients over different scales. The top panel shows the original electron density (2 Hz) in blue, and the linear fits of the intervals centred at 18:21.40 universal time (UT) are shown in green, black and red dashed lines. The bottom panel shows the density gradients calculated in respective running windows.

where $\overline{\text{ROD}}$ is the mean value of $\text{ROD}(t_i)$:

$$\overline{\text{ROD}} = \frac{1}{N} \sqrt{\sum_{t_i=t-\Delta t/2}^{t_i=t+\Delta t/2} \text{ROD}(t_i)}, \quad (3)$$

where we use $\Delta t = 10\text{s}$ for RODI10s, and $\Delta t = 20\text{s}$ for RODI20s.

Finally, parameters Δn_{e10s} , Δn_{e20s} , Δn_{e40s} (i.e., delta_Ne10s, delta_Ne20s, delta_Ne40s), correspond to the amplitudes of plasma fluctuations, and are obtained by subtracting the median filtered value of n_e in $\Delta t = 10, 20$ and 40s from the actual value of n_e . These scales correspond to fluctuations at scales smaller than 75, 150 and 300 km, respectively.

The electron density, electron temperature, and derived electron density parameters are down-sampled to 1 Hz. This is to make these parameters compatible with the total electron content (TEC) of the topside ionosphere data entries, which are nominally provided at 1Hz for the Swarm mission.

The TEC data are derived based on TECxTMS_2F dataset. We use the threshold elevation angle of 30 degrees to ensure that the TEC data correspond to local plasma conditions. mVTEC is the median of the vertical TEC from all satellites above the threshold elevation angle. For characterising fluctuations in TEC we use the rate of change of TEC (ROT) and the rate of change of TEC index (ROTI). These are defined in analogous way as ROD and RODI:

$$\text{ROT}(t) = \frac{\text{TEC}(t + \Delta t) - \text{TEC}(t)}{\Delta t}, \quad (4)$$

and

$$\text{ROTI}(t) = \sqrt{\frac{1}{N-1} \sum_{t_i=t-\Delta t/2}^{t_i=t+\Delta t/2} |\text{ROT}(t_i) - \overline{\text{ROT}}|^2}, \quad (5)$$

where $\overline{\text{ROT}}$ is the mean value of $\text{ROT}(t_i)$:

$$\overline{\text{ROT}} = \frac{1}{N} \sqrt{\sum_{t_i=t-\Delta t/2}^{t_i=t+\Delta t/2} \text{ROT}(t_i)}, \quad (6)$$

with $\Delta t = 10\text{s}$ for mROTI10s, and $\Delta t = 20\text{s}$ for mROTI20s. For calculating TEC related parameters again the threshold value of the elevation angle of 30 degrees is used and the median values are provided.

For completeness, the plasma bubble index (IBI_flag) is provided directly from the IBIXTMS_2F dataset (Park et al., 2013).

An important aspect of the IPIR dataset is that it assigns the plasma variations to different geomagnetic regions in parameter `Ionosphere_region_flag`: equatorial region (0), mid-latitudes (1), auroral oval (2), and the polar cap (3). This allows the user to perform larger statistical studies in relation to processes in these different regions. The equatorial region is defined between $\pm 30^\circ$ of the magnetic latitude (MLAT). Here the magnetic latitude is calculated with quasi-dipole coordinates (Emmert et al., 2010; Richmond, 1995), in accordance with previous studies (Park et al., 2010). Mid-latitudes are poleward of the equatorial region and the equatorward auroral oval boundary (AOB). AOBs are determined dynamically, by detecting the small-scale signatures of the field-aligned currents (FACs) from the Swarm magnetic field data (Xiong et al., 2014; Xiong & Lühr, 2014). While the estimates of FAC are derived routinely based on single spacecraft data (provided in FACxTMS_2F), in IPIR we use the small-scale ($< 10\text{km}$) FAC part of the data product, in which the auroral boundaries can be sharply detected. The auroral boundaries are based on the maxima and gradients in the FACs' intensity. The poleward and equatorward AOBs correspond to the middle of the linear part of the corresponding gradients from the maximum of the FAC intensity. We note that sometimes no FACs are detected, for example, due to a combination of the orbital characteristics and the level of geomagnetic activity, and in such cases, AOBs are not determined. The polar cap region is defined as poleward from the poleward AOBs, or if they are not detected, poleward of 77° MLAT, consistent with the Polar Cap Products. Thus the auroral region is defined as between $65 - 77^\circ$ MLAT.

4.1 IPIR index

The IPIR index is evaluated based on the characteristics of the fluctuations in the plasma density. The IPIR index is a product of RODI10s and the standard deviation of Δn_{e10s} (i.e., of Δn_{e10s}):

$$\text{IPIR}_{\text{ix}} = \text{RODI10s} \cdot A(n_e)_{10s}, \quad (7)$$

where $A(n_e)_{10s}$ is the standard deviation of Δn_{e10s} in a running window of 10 seconds:

$$A(n_e)_{10s}(t) = \sqrt{\frac{1}{N-1} \sum_{t_i=t-\Delta t/2}^{t_i=t+\Delta t/2} |\Delta n_{e10s}(t_i) - \overline{\Delta n_{e10s}}|^2}, \quad (8)$$

where $\overline{\Delta n_{e10s}}$ is the mean value of $\Delta n_{e10s}(t_i)$ in this time interval:

$$\overline{\Delta n_{e10s}} = \frac{1}{N} \sum_{t_i=t-\Delta t/2}^{t_i=t+\Delta t/2} \Delta n_{e10s}(t_i), \quad (9)$$

As mentioned earlier, RODI10s is the variance of fluctuations (gradients at small scales) in density, which indicates structuring of plasma within the 10 seconds interval. $A(n_e)_{10s}$ is related to the absolute amplitudes of fluctuations within the 10 seconds interval. The correlation between these two parameters is weak, and their combination can provide indication about the intensity of structuring of ionospheric plasma, where the high frequency fluctuations with large amplitudes are giving highest numerical values of IPIR_{ix}. The following IPIR_{ix} index scale has been provided corresponding to level of fluctuations in the ionospheric plasma density: 0 – 3 (low), 4 – 5 (medium), and > 6 (high). The scale corresponds to the numerical values of IPIR_{ix} differing by an order of magnitude, where index value 1 in the dataset corresponds to $\text{IPIR}_{ix} < 10^3 \text{cm}^{-3} \text{s}^{-1} \text{cm}^{-3}$, index value 2 corresponds to $\text{IPIR}_{ix} \in (10^3 - 10^4) \text{cm}^{-3} \text{s}^{-1} \text{cm}^{-3}$, index value 3 corresponds to $\text{IPIR}_{ix} \in (10^4 - 10^5) \text{cm}^{-3} \text{s}^{-1} \text{cm}^{-3}$, etc.

High values of IPIR_{ix} are potentially leading to stronger space weather effects. In Fig. 2 we demonstrate the relationship between IPIR_{ix} and phase scintillation index measured at high latitudes. While there is no linear relationship, it is clear that the values of the phase scintillation index increase with increasing IPIR_{ix}. Larger IPIR_{ix} also relate to the increase in the minimal observed phase scintillation levels. The work on quantifying the relationship between IPIR_{ix} and ground-based observations of scintillation of trans-ionospheric waves is ongoing. However, we note that this relationship is nontrivial: Swarm does not access scales that are responsible for scintillations of the GNSS signals (i.e., hectometer scales), the conjunction times are relatively short, and the in situ Swarm measurements are in the upper F-layer of the ionosphere. Orientation of the magnetic field (horizontal at low latitudes vs. vertical at high latitudes), low statistics, and locality of events make evaluation of such a relationship a challenging study. Thus, a scintillation observed on the ground does not need to be reflected in the Swarm data. On the other hand, highly structured plasma observed by Swarm may indicate that scintillations occur, provided that plasma structuring goes down to hectometer scales.

5 Example of use

An example of use and applicability of the IPIR dataset is shown in Figures 3 and 4. Here we show results for the Swarm A satellite half-orbits on September 8, 2017, during daytime (Fig. 3) and nighttime (Fig. 4). The Swarm A trajectories are shown in panels (a) of the figures, where they are over-plotted on the global ionosphere map (GIM) produced by the Center for Orbit Determination in Europe (CODE) using global distributed ground-based GNSS receivers (Jee et al., 2010; Schaer, 1999).

In the top rows of Figures 3(b) and 4(b), we plot the actual electron plasma density, n_e , as well as background density and electron temperature. The bottom panels show PCP/IBI indices together with ionosphere region flag. We see that during daytime, there is a significant increase in the background density at equatorial regions, low density at mid-latitudes, and some enhanced density in the polar regions on the dayside (Fig. 3). At the pre-midnight time, the ESF is seen in the depleted density and enhanced temperature at low latitudes (Fig. 4).

The second panels show the ROD and RODI in 10s and 20s. There is a consistent high structuring in the polar regions, which is related to the polar cap patches. Smaller structuring is also observed in the auroral oval. On the nightside significant plasma irregularities are present at low latitudes which correspond to plasma bubbles in the equatorial region (Smith & Heelis, 2017).

The field-aligned currents and corresponding AOBs are presented in the same panel. The auroral oval has a large extent on the nightside (Fig. 4), which can be associated with the nighttime auroral activity, but at the same time, the corresponding

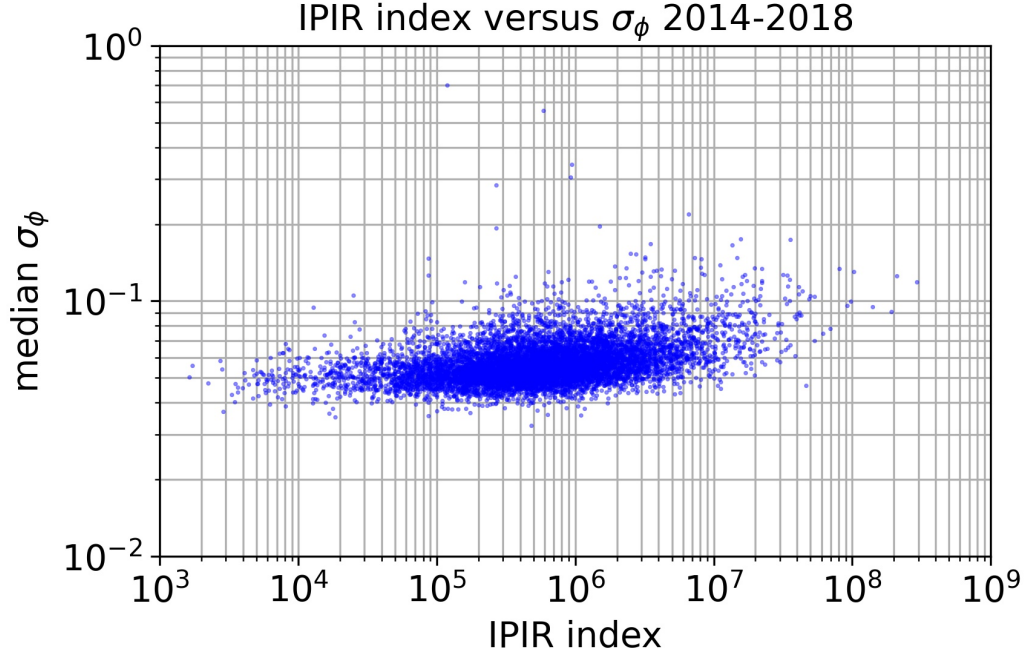


Figure 2. Relationship between the IPIR index numerical values and the median phase scintillation index observed at Ny-Ålesund for 2014-2018 period. The phase scintillation index has been obtained with the GSV-4004B receiver operated by the University of Oslo.

plasma is not subject to significant structuring. However, the dayside auroral oval is narrow (Fig. 3), and in the southern hemisphere, it is also significantly structured, which can be associated with the cusp region. In general, the plasma in the southern polar cap is more structured than in the northern hemisphere.

The four remaining panels show mVTEC and ROTI, fluctuation amplitudes Δn_e over the baseline over 10/20/40s, and gradients in the electron density over 20/50/100 km, respectively. The parameters derived from the topside ionosphere TEC are consistent with the parameters derived from density. There is a good correlation between Δn_e and ROD/RODI measurements. Presented parameters make it possible to estimate the scale of plasma structures along the satellite pass.

In the above example, we observed typical structures in the ionosphere and could assess their variability. IPIR dataset can provide comprehensive characteristics of plasma density structuring along the Swarm satellites' orbits. Having different parameters in a single dataset facilitates a detailed study of particular events, but also allows for larger systematic studies.

The IPIR dataset has already been used in addressing the structuring of plasma at high latitudes. The climatological study revealed interhemispheric asymmetry in plasma structuring, with more pronounced and widely distributed irregularities in the southern hemisphere, whereas in the northern hemisphere the plasma irregularities are commonly attributed to the cusp region and the nighttime auroral oval (Jin et al., 2019; Jin & Xiong, 2020). Several years of data revealed seasonal characteristics of the irregularities in the plasma density, where also clear dependence on the solar activity was demonstrated for the declining phase of the solar cycle. In another study, the global distribution of irregularities was studied, and the results of the in situ measure-

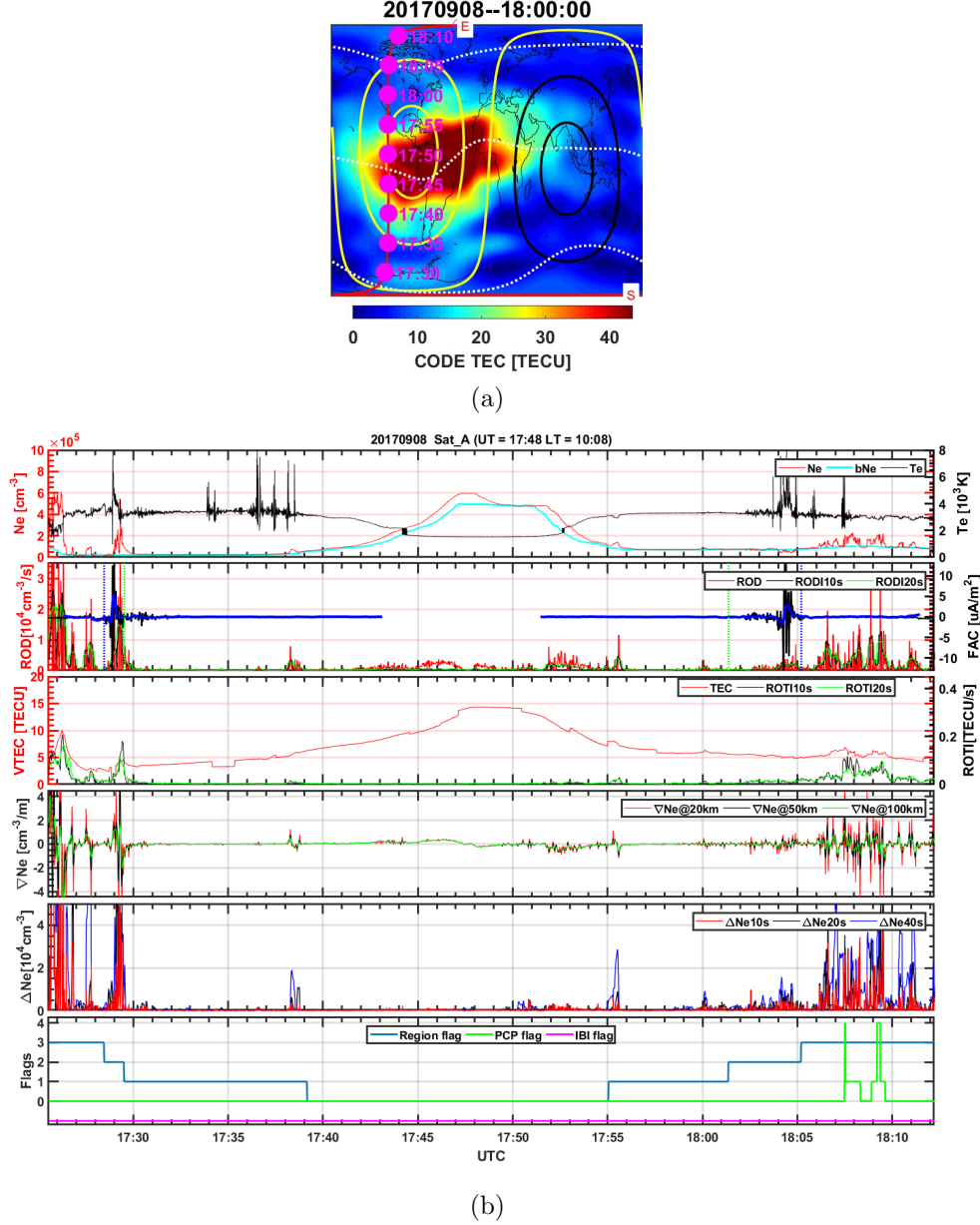


Figure 3. Example of the IPIR parameters along the orbit of Swarm A satellite on September 8, 2017 at 17:25–18:12 UT corresponding to local daytime (17:48 UT corresponds to 10:08 LT). (a) The Swarm trajectory on the global TEC map obtained from the Madrigal database ⁵. (b) The corresponding IPIR parameters: The top panel shows the actual electron plasma density (red line), n_e , background density (blue line) and electron temperature (black line). The second panel shows ROD (red), RODI10s (black), RODI20s (green) along with FAC (blue with black lines, Y axis scale is on the right). The vertical dashed lines show the equatorial (green) and poleward (blue) edges of the auroral oval, respectively. The third panel shows data from GPSR: mVTEC (red), ROTI10s (black) and ROTI20s (green). The fourth panel shows the electron density gradient over 20 km (red), 50 km (black) and 100 km (green). The next panel shows Δn_{e10s} (red), Δn_{e20s} (black), and Δn_{e40s} (blue). The bottom panel shows PCP/IBI indices together with the ionosphere region flag.

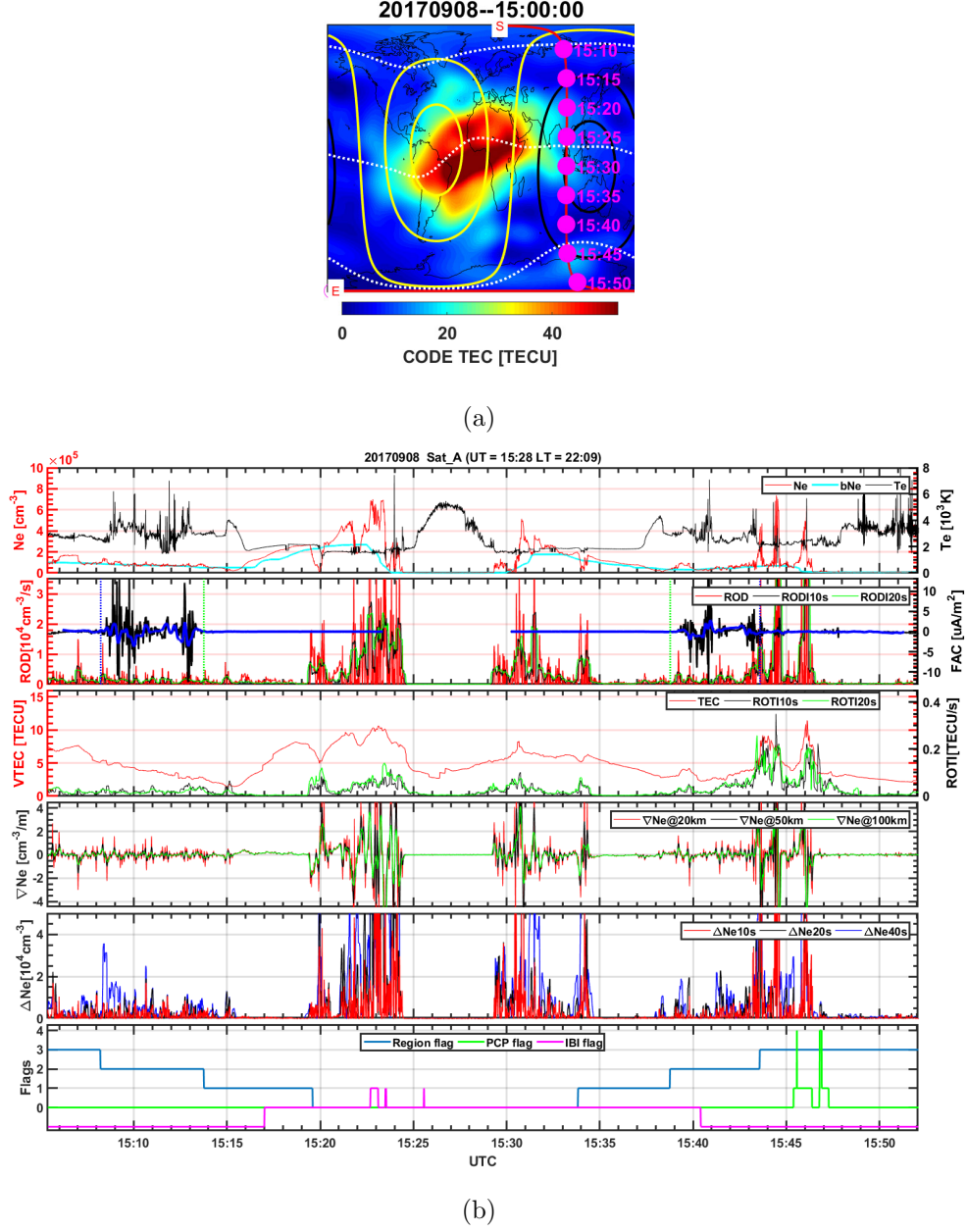


Figure 4. As in Fig. 3, but for the orbit of Swarm A satellite on September 8, 2017 at 15:05–15:52 UT, corresponding to local nighttime (15:28 UT corresponds to 22:09 LT).

ments by Swarm were in agreement with the scintillation distribution observed on the ground (Jin et al., 2020). Several years of data so far from the Swarm mission opens a possibility for climatology studies and for addressing distributions of ionospheric plasma parameters, which can, in turn, be used for ionospheric models that would account for ionospheric plasma variability and structuring (Kotova et al., 2021).

6 Conclusions

The IPIR dataset has been developed to provide comprehensive characteristics of structuring in ionospheric plasma along trajectories of the Swarm satellites. The measurements are categorised according to geomagnetic regions. The dataset includes in situ measurements of the plasma density as well as the total electron content of the topside ionosphere, and derived parameters. IPIR dataset is freely accessible through the ESA dissemination server, as well as through an interactive VirEs for Swarm visualisation tools. It opens possibility both for detailed case studies of the processes in the ionosphere, and for long-term global statistical studies of ionospheric plasma structuring and variability.

Acknowledgments

The IPIR dataset has been developed within the Swarm DISC—Data, Innovation, and Science Cluster, funded through the European Space Agency, through ESA contract 4000109587/13/I-NB, as a part of the Agency’s Earth Observation Envelope Programme (EOEP). The work is partially supported by the Research Council of Norway under grants 267408, 275655, and 275653. WJM acknowledges support from the European Research Council (ERC) under the European Unions Horizon 2020 research and innovation programme (ERC CoG grant agreement No 866357). This work is also part of the 4DSpace Strategic Research Initiative at the University of Oslo. The GPS TEC data for GPS TEC map in Figures 3 and 4 can be obtained through the CODE GIM data (from <ftp://ftp.aiub.unibe.ch/CODE/>). The IPIR dataset is available at <https://swarm-diss.eo.esa.int>, and the reference documentation can be found at <https://earth.esa.int/web/guest/missions/esa-eo-missions/swarm/key-documentation>.

References

- Basu, S., Groves, K. M., Basu, S., & Sultan, P. J. (2002). Specification and forecasting of scintillations in communication/navigation links: current status and future plans. *J. Atmos. Sol-Terr. Phys. (UK)*, **64**(16), 1745–1754. doi: 10.1016/S1364-6826(02)00124-4
- Basu, S., MacKenzie, E., & Basu, S. (1988). Ionospheric constraints on VHF/UHF communications links during solar maximum and minimum periods. *Radio Science*, **23**(3), 363–378. doi: <https://doi.org/10.1029/RS023i003p00363>
- Borovsky, J. E. (2021). Is our understanding of solar-wind/magnetosphere coupling satisfactory? *Frontiers in Astronomy and Space Sciences*, **8**, 5. Retrieved from <https://www.frontiersin.org/article/10.3389/fspas.2021.634073> doi: 10.3389/fspas.2021.634073
- Buchert, S., Zangerl, F., Sust, M., André, M., Eriksson, A., & Wahlund, J. E. (2015). Swarm observations of equatorial electron densities and topside GPS track losses. *Geophys. Res. Lett.*, **42**(7), 2088–2092. doi: 10.1002/2015GL063121
- Carlson, H. C. (2012). Sharpening our thinking about polar cap ionospheric patch morphology, research, and mitigation techniques [Journal Article]. *Radio Science*, **47**. Retrieved from <GotoISI>://WOS:000304773200002 doi: 10.1029/2011rs004946
- Cowley, S., & Lockwood, M. (1992). Excitation and decay of solar wind-driven flows

- in the magnetosphere-ionosphere system. In *Annales geophysicae* (Vol. 10, pp. 103–115).
- Crowley, G. (1996). Critical review of ionospheric patches and blobs. In W. Stone (Ed.), *Review of Radio Science 1993–1996* (pp. 619–648). New York: Oxford Univ. Press.
- Emmert, J. T., Richmond, A. D., & Drob, D. P. (2010). A computationally compact representation of magnetic-apex and quasi-dipole coordinates with smooth base vectors [Journal Article]. *Journal of Geophysical Research-Space Physics*, 115. Retrieved from <GotoISI>://WOS:000281417700009 doi: 10.1029/2010ja015326
- Farley, D. T., Balsey, B. B., Woodman, R. F., & McClure, J. P. (1970). Equatorial spread F: Implications of VHF radar observations [Journal Article]. *Journal of Geophysical Research (1896-1977)*, 75(34), 7199–7216. Retrieved from <https://agupubs.onlinelibrary.wiley.com/doi/abs/10.1029/JA075i034p07199> doi: 10.1029/JA075i034p07199
- Friis-Christensen, E., Lühr, H., & Hulot, G. (2006). Swarm: A constellation to study the Earth's magnetic field. *Earth, Planets Space*, 58(4), 351–358. doi: 10.1186/BF03351933
- Hasegawa, H., Fujimoto, M., Phan, T.-D., Rème, H., Balogh, A., Dunlop, M. W., ... TanDokoro, R. (2004). Transport of solar wind into Earth's magnetosphere through rolled-up Kelvin–Helmholtz vortices. *Nature*, 430, 755–758. doi: <https://doi.org/10.1038/nature02799>
- Jakowski, N., Beniguel, Y., De Franceschi, G., Pajares, M. H., Jacobsen, K. S., Stanislawska, I., ... Wautelet, G. (2012). Monitoring, tracking and forecasting ionospheric perturbations using GNSS techniques [Journal Article]. *Journal of Space Weather and Space Climate*, 2, 14. Retrieved from <GotoISI>://WOS:000325007800022 doi: UNSPA2210.1051/swsc/2012022
- Jakowski, N., Stankov, S. M., & Klaehn, D. (2005). Operational space weather service for GNSS precise positioning. *Annales Geophysicae*, 23(9), 3071–3079. Retrieved from <https://angeo.copernicus.org/articles/23/3071/2005/> doi: 10.5194/angeo-23-3071-2005
- Jee, G., Lee, H.-B., Kim, Y. H., Chung, J.-K., & Cho, J. (2010). Assessment of GPS global ionosphere maps (gim) by comparison between code gim and TOPEX/Jason TEC data: Ionospheric perspective. *Journal of Geophysical Research: Space Physics*, 115(A10). Retrieved from <https://agupubs.onlinelibrary.wiley.com/doi/abs/10.1029/2010JA015432> doi: <https://doi.org/10.1029/2010JA015432>
- Jin, Y., Moen, J. I., & Miloch, W. J. (2014). GPS scintillation effects associated with polar cap patches and substorm auroral activity: direct comparison. *J. Space Weather Space Clim.*, 4, A23. Retrieved from <https://doi.org/10.1051/swsc/2014019> doi: 10.1051/swsc/2014019
- Jin, Y., Moen, J. I., & Miloch, W. J. (2015). On the collocation of the cusp aurora and the GPS phase scintillation: A statistical study [Journal Article]. *Journal of Geophysical Research-Space Physics*, 120(10), 9176–9191. Retrieved from <GotoISI>://WOS:000366135200073 doi: 10.1002/2015ja021449
- Jin, Y., Moen, J. I., Miloch, W. J., Clausen, L. B. N., & Oksavik, K. (2016). Statistical study of the GNSS phase scintillation associated with two types of auroral blobs [Journal Article]. *Journal of Geophysical Research-Space Physics*, 121(5), 4679–4697. Retrieved from <GotoISI>://WOS:000380025500058 doi: 10.1002/2016ja022613
- Jin, Y., Moen, J. I., Spicher, A., Oksavik, K., Miloch, W. J., Clausen, L. B. N., ... Saito, Y. (2019). Simultaneous rocket and scintillation observations of plasma irregularities associated with a reversed flow event in the cusp ionosphere. *Journal of Geophysical Research: Space Physics*, 124(8), 7098–7111. doi: 10.1029/2019ja026942

- Jin, Y., & Xiong, C. (2020). Interhemispheric asymmetry of large-scale electron density gradients in the polar cap ionosphere: UT and seasonal variations [Journal Article]. *Journal of Geophysical Research: Space Physics*, *125*(2), e2019JA027601. Retrieved from <https://agupubs.onlinelibrary.wiley.com/doi/abs/10.1029/2019JA027601> doi: 10.1029/2019ja027601
- Jin, Y., Xiong, C., Clausen, L., Spicher, A., Kotova, D., Brask, S., ... Miloch, W. (2020). Ionospheric plasma irregularities based on in situ measurements from the Swarm satellites. *J. Geophys. Res.: Space Phys.*, *125*(7), e2020JA028103. doi: 10.1029/2020JA028103
- Kintner, P. M., Ledvina, B. M., & De Paula, E. R. (2007). GPS and ionospheric scintillations [Journal Article]. *Space Weather-the International Journal of Research and Applications*, *5*(9). Retrieved from <GotoISI>://WOS:000253075400001 doi: 10.1029/2006sw000260
- Kintner, P. M., & Seyler, C. E. (1985). The status of observations and theory of high latitude ionospheric and magnetospheric plasma turbulence [Journal Article]. *Space Science Reviews*, *41*(1), 91-129. Retrieved from <https://doi.org/10.1007/BF00241347> doi: 10.1007/BF00241347
- Knudsen, D. J., Burchill, J. K., Buchert, S. C., Eriksson, A. I., Gill, R., Wahlund, J. E., ... Moffat, B. (2017). Thermal ion imagers and Langmuir probes in the Swarm electric field instruments. *J. Geophys. Res.: Space Phys.*, *122*(2), 2655–2673. doi: 10.1002/2016JA022571
- Kotova, D., Jin, Y., & Miloch, W. J. (2021). Interhemispheric variability of the electron density and derived parameters by the swarm satellites during different solar activity. submitted, .
- Lockwood, M., & Carlson, H. C. (1992). Production of polar cap electron density patches by transient magnetopause reconnection. *Geophys. Res. Lett.*, *19*(17), 1731–1734. doi: 10.1029/92GL01993
- Lühr, H., Park, J., Gjerloev, J. W., Rauberg, J., Michaelis, I., Merayo, J. M. G., & Brauer, P. (2015). Field-aligned currents' scale analysis performed with the Swarm constellation. *Geophys. Res. Lett.*, *42*(1), 1–8. doi: 10.1002/2014GL062453
- Moen, J., Oksavik, K., Alfonsi, L., Daabakk, Y., Romano, V., & Spogli, L. (2013). Space weather challenges of the polar cap ionosphere [Journal Article]. *Journal of Space Weather and Space Climate*, *3*. Retrieved from <GotoISI>://WOS:000330569100003 doi: 10.1051/swsc/2013025
- Olsen, N., Friis-Christensen, E., Floberghagen, R., Alken, P., Beggan, C. D., Chuliat, A., ... van den Ijssel, J. (2013). The Swarm satellite constellation application and research facility (SCARF) and Swarm data products. *Earth, Planets Space*, *65*(11), 1189–1200. doi: 10.5047/eps.2013.07.001
- Park, J., Lühr, & Min, K. (2010). Neutral density depletions associated with equatorial plasma bubbles as observed by the champ satellite. *J. Atm. Sol.-Terr. Phys.*, *72*(2-3), 157-163.
- Park, J., Noja, M., Stolle, C., & Lühr, H. (2013). The Ionospheric Bubble Index deduced from magnetic field and plasma observations onboard Swarm. *Earth, Planets and Space*, *65*, 13. doi: 10.5047/eps.2013.08.005
- Pi, X., Mannucci, A. J., Lindqwister, U. J., & Ho, C. M. (1997). Monitoring of global ionospheric irregularities using the worldwide GPS network. *Geophys. Res. Lett.*, *24*(18), 2283–2286. doi: 10.1029/97GL02273
- Richmond, A. D. (1995). Ionospheric electrodynamics using magnetic apex coordinates [Journal Article]. *Journal of Geomagnetism and Geoelectricity*, *47*(2), 191-212. Retrieved from <GotoISI>://WOS:A1995QY49900004 doi: DOI10.5636/jgg.47.191
- Ritter, P., Lühr, H., & Rauberg, J. (2013). Determining field-aligned currents with the Swarm constellation mission. *Earth, Planets Space*, *65*(11), 1285–1294. doi: 10.5047/eps.2013.09.006

- Rodríguez-Zuluaga, J., Stolle, C., & Park, J. (2017). On the direction of the Poynting flux associated with equatorial plasma depletions as derived from Swarm. *Geophysical Research Letters*, *44*(12), 5884–5891.
- Schaer, S. (1999, January). Mapping and predicting the Earth’s ionosphere using the Global Positioning System. *Geod.-Geophys. Arb. Schweiz*, *59*.
- Smith, J., & Heelis, R. A. (2017). Equatorial plasma bubbles: Variations of occurrence and spatial scale in local time, longitude, season, and solar activity. *Journal of Geophysical Research: Space Physics*, *122*(5), 5743–5755. doi: <https://doi.org/10.1002/2017JA024128>
- Spicher, A., Cameron, T., Grono, E. M., Yakymenko, K. N., Buchert, S. C., Clausen, L. B. N., ... Moen, J. I. (2015). Observation of polar cap patches and calculation of gradient drift instability growth times: A Swarm case study. *Geophys. Res. Lett.*, *42*(2), 201–206. doi: 10.1002/2014GL062590
- Spicher, A., Clausen, L. B. N., Miloch, W. J., Lofstad, V., Jin, Y., & Moen, J. I. (2017). Interhemispheric study of polar cap patch occurrence based on Swarm in situ data. *J. Geophys. Res.: Space Phys.*, *122*(3), 3837–3851. doi: 10.1002/2016JA023750
- Stolle, C., Floberghagen, R., Lühr, H., Maus, S., Knudsen, D. J., Alken, P., ... Visser, P. N. (2013). Space weather opportunities from the Swarm mission including near real time applications. *Earth Planets Space*, *65*(11), 1375–1383. doi: 10.5047/eps.2013.10.002
- van der Meeren, C., Oksavik, K., Lorentzen, D. A., Rietveld, M. T., & Clausen, L. B. (2015). Severe and localized GNSS scintillation at the poleward edge of the nightside auroral oval during intense substorm aurora [Journal Article]. *Journal of Geophysical Research: Space Physics*, *120*(12), 10,607–10,621.
- Wood, A. G., & et al. (2021). Variability of ionospheric plasma: Results from the ESA Swarm Mission. submitted.
- Woodman, R. F. (2009). Spread F – an old equatorial aeronomy problem finally resolved? *Annales Geophysicae*, *27*(5), 1915–1934. doi: 10.5194/angeo-27-1915-2009
- Woodman, R. F., & La Hoz, C. (1976). Radar observations of f region equatorial irregularities [Journal Article]. *Journal of Geophysical Research (1896-1977)*, *81*(31), 5447–5466. Retrieved from <https://agupubs.onlinelibrary.wiley.com/doi/abs/10.1029/JA081i031p05447> doi: 10.1029/JA081i031p05447
- Xiong, C., & Lühr, H. (2014). An empirical model of the auroral oval derived from CHAMP field-aligned current signatures, part 2. *Annales Geophysicae*, *32*(6), 623–631. Retrieved from <https://angeo.copernicus.org/articles/32/623/2014/> doi: 10.5194/angeo-32-623-2014
- Xiong, C., Lühr, H., Wang, H., & Johnsen, M. G. (2014). Determining the boundaries of the auroral oval from CHAMP field-aligned current signatures; part 1. *Annales Geophysicae*, *32*(6), 609–622. Retrieved from <https://angeo.copernicus.org/articles/32/609/2014/> doi: 10.5194/angeo-32-609-2014
- Xiong, C., Stolle, C., & Park, J. (2018). Climatology of GPS signal loss observed by Swarm satellites. In *Ann. Geophys. (Vol. 36, pp. 679–693)*. doi: 10.5194/angeo-36-679-2018